Novel method to determine the actual surface area of a laser-nanotextured sensor

Ričardas Buividas[1]*, Narges Fahim[1], Jurga Juodkazytė[2], Saulius Juodkazis[1†]

September 18, 2013

Abstract

The actual surface area of a gold-coated conductive layer over the laser nano-textured surface of sapphire is determined using an electrochemical cyclic voltammetry. The method is down scaled to measure the sensing surface area of 200×200 μm^2 on a laser-ablated ripple sensor used for surface-enhanced Raman spectroscopy/scattering (SERS). Ripple SERS sensors made on different substrates of high refractive index materials: GaP, diamond, SiC, and Al_2O_3 make a versatile sensing platform with detection of analyte (here a thiophenol) down to 10 nM concentrations.

Direct measurement of the surface area provides a powerful tool to investigate roughness, porosity, and morphology of coatings used for SERS or other light harvesting surfaces such as solar cells. Novelty of the proposed method is in use of cathodic peak of surface passivation-activation cycle for calculation of surface charge. The method enables high-accuracy surface area measurements from as small as 0.01 mm^2 pads up to functional solar cells.

1 Introduction

Determination of the actual (real) surface area is a key requirement for analysis of different processes ranging from solar energy harvesting, fuel cells, hydrogen evolution and storage electrodes, and in various sensing applications [1–3]. In surface enhanced Raman scattering (SERS) [4], the area occupied by hot spots [5] where light intensity is enhanced has to be determined in order to make quantitative estimations of the light enhancement factors [6–10]. This is achievable for the lithographically defined nanoparticles and their patterns [11, 12],

*ricardas.buividas@gmail.com

†[1]Centre for Micro-Photonics and The Australian National Fabrication Facility – ANFF, Victoria node, Faculty of Engineering and Industrial Sciences, Swinburne University of Technology, Hawthorn, VIC 3122, Australia, [2] Center for Physical Sciences and Technology, Institute of Chemistry, A. Goštauto 9, Vilnius LT-01108, Lithuania [3] Faculty of Engineering and Industrial Sciences, Swinburne University of Technology, Hawthorn, VIC 3122, Australia

however, more practical applications implement patterns of random nanoparticles [13] or nanotextured [14] surfaces. Hot-spots on nano-rough films of Au or Ag are expected to be dependent on the porosity, formation of nano-grooves, bumps, crevices which can guide or scatter light. Hence, morphology of sensing films at nanoscale revealed via the electrochemical measurement of the actual surface area will help to understand light field enhancement at the required microscopic level.

The ideal surface area of a metal electrode is defined by the surface number density of atoms. In electrochemistry evaluation of the real surface area of the electrode is usually based on the measurement of charge required for the adsorption/formation or desorption/removal of a monolayer of some atoms or ions (most often H, O, Tl, etc). To obtain the surface increase factor, f_{si}, experimentally measured surface charge, Q_r, on a corrugated real surface is divided by the experimentally or theoretically determined *monolayer* charge $Q_{exp,t}$, respectively, which is required to deposit a monolayer of surface-bound oxygen or hydrogen on the atomically "flat"ideal electrode of a given geometrical footprint (or projected area) S_g [15]:

$$f_{si} = \frac{S_r}{S_g} = \frac{Q_r}{Q_{exp,t}} = \frac{Q_r}{\sigma_{exp,t} S_g}, \tag{1}$$

where $\sigma_{exp,t}$ is the experimentally or theoretically determined charge density. The value $\sigma_{exp} = 0.4$ mC/cm^2 was considered to correspond to formation of a monolayer of oxygen atoms on a polycrystalline surface of a gold electrode [16]; this corresponds to the *atom denisty* $\times\, e \times 2$; where e is the electron charge and factor 2 accounts for two electrons required for oxygen deposition on surface according to the overall reaction $H_2O{-}2e \leftrightarrows O + 2H^+$ [16]. For the hydrogen monolayer deposition on the Pt electrode $\sigma_{exp} = 0.208$ mC/cm^2 [15], since only one electron exchange occurs according to $H^+ + e \leftrightarrows H$.

Here, we demonstrate a method of surface area measurement of a laser ablated surface - ripples - on sapphire coated by gold. The method is based on a more sensitive detection of the charge exchange on the electrode in the cathodic region of a voltammetric cycle. The reference theoretical surface density, and related theoretical surface charge density $\sigma_t \simeq 0.48$ mC/cm^2, of Au atoms was calculated from geometrical lattice parameters. It is demonstrated, that very small surface areas down to 0.01 mm^2 can be measured with high accuracy ∼95%. Areas of ripple sensor of $S_g = 200 \times 200$ μm^2 were measured and compared with SERS intensity increase.

2 Experimental

2.1 Improved surface area measurement

The electrolyte of 0.5 M H_2SO_4 was deaerated by N_2 before and during experiments. Autolab potentiostat/galvanostat was used to measure cyclic voltammograms. Working electrodes, WE, were a Au-coated ripples on sapphire, flat

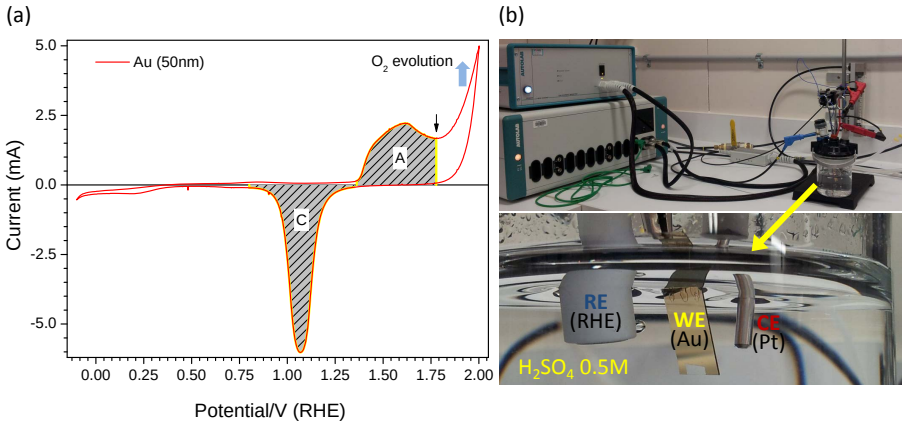

Figure 1: (a)Typical cyclic voltammetry of a Au thermally deposited on a cover glass; thickness of Au is 50 nm. *Anodic* and *Cathodic* peaks are marked. The arrow shows the Burshtein minimum, before the oxygen evolution onset at a more positive bias. The voltage scan rate was $v = 0.1$ V/s, geometrical area of the immersed WE was $S_g = 4.0$ cm^2. (b)Photo shows photo of the measurement setup, image below shows connections of the working (WE), reference (RE), and counter (CE) electrodes when immersed in electrolyte; the reference hydrogen electrode is denoted RHE.

sapphire and flat cover glass with a geometrical surface area S_g immersed into electrolyte. The counter electrode, CE, was Pt and the reference electrode, RE, was the hydrogen electrode in a working solution (RHE) since it is not contaminating the electrolyte [15]. In most experiments, the voltage scan rate was $v = 0.01$ V/s. It was important to set a slow scan rate for the small area measurements, e.g., the current was too noisy at $v = 0.05$ V/s for $S_t = 0.01$ mm^2. The relation between the potential of RHE and the standard hydrogen electrode, SHE, is given by $E_{RHE} = E_{SHE} - 0.059pH$. When using a 0.5 M solution of H_2SO_4 with $pH \approx 0$, $E_{RHE} \approx E_{SHE}$, therefore SHE and RHE scales are practically the same.

Usually, the anodic charge Q_a, which is considered to correspond to the monolayer of adsorbed O atoms [17], is calculated from the onset of surface modification at potential $E_1 \simeq 1.36$ V till the Burshtein minimum $E_2 \simeq 1.78$ V (the onset point of oxygen evolution [16]; Fig. 1) and can be slightly affected by the distance between electrodes which will be reflected by ohmic losses in solution. The charge is integrated as

$$Q = \int_{E_1}^{E_2} IdE/v, \tag{2}$$

where v is the voltage scan rate.

Since the potential of the Burshtein minimum has ambiguity in its deter-

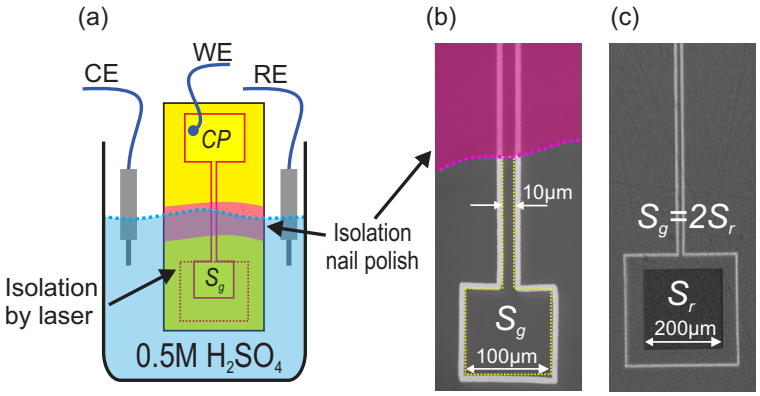

Figure 2: Real surface area measurement. (a) An illustration of a gold coated, laser patterned glass substrate immersed into electrolyte; electrode connections, active measurement area S_g and contact pad CP indicated. (b) An optical microscope image of a $S_g \approx 0.01$ mm^2 area, isolated by laser ablation and nail polish. (c) Ripples, fabricated in a $S_r \approx 0.04$ mm^2 area, isolated by a two times larger $S_g = 2 \times S_r \approx 0.08$ mm^2 area.

mination, moreover the charge Q_a is a function of time [18], we introduce here a new method of charge determination from the *Cathodic* peak, the origin of which (Fig. 1) is reduction of surface layer of $Au(OH)_3$ [19, 20]. First, voltage is set close to the Burshtein minimum and kept for 5 min for current to drop to zero as a passivation layer is formed (presumably a monolayer of $Au(OH)_3$) on the electrode. Then, the passivation layer is reduced by scanning potential to 0 V and the obtained *Cathodic* peak is used to calculate the real surface charge $Q_r = Q_c$ by integration (Eq. 2) over the *Cathodic* peak (Fig. 1). The actual surface area is obtained by $S_r = S_g \times f_{si}$, where surface increase (mainly due to augmented surface roughness) factor f_{si} is calculated using Eq. 1. For calculations here, the theoretical surface charge density $\sigma_t = 0.483$ mC/cm^2 is considered (see details below), which is slightly larger than used for the anodic method of charge calculations with $\sigma_{exp} = 0.4$ mC/cm^2 [16].

Formation of Au nanocrystallites contributes to an increase of the actual surface area. It is instructive to define the ideal surface area of an electrode on the pure geometrical parameters of the Au lattice [21]. Polycrystalline Au is usually assumed to consist of equal $\frac{1}{3}$ fractions [22] of the low index Miller planes (100), (110), and (111). Hence, for a single crystalline plane a surface density of the available adsorption sites would slightly vary for different planes $[\frac{atoms}{area}]$: $\frac{2}{a^2}$ for (100), $\frac{1}{a^2\sqrt{2}}$ for (110), and $\frac{2}{a^2(\sqrt{3}/2)}$ for (111), here $a = 0.408$ nm is the face-centered-cubic (fcc) crystal lattice period of Au. The average number of Au surface atoms available for oxidation is $\varphi_s = 1.005 \times 10^{15}$ atoms/cm^2 which corresponds to the $\varphi_s/N_a = 1.668$ nmol/cm^2 molar surface density of gold; N_a

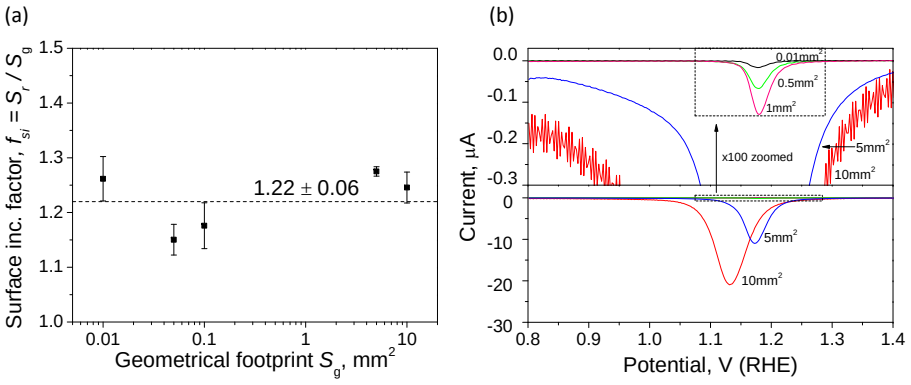

Figure 3: (a) The surface increase factor for a 30 nm Au on glass for different geometrical footprint S_g. Error bars indicate standard deviation between three samples of the same S_g value. (b) Cathodic peak of a cyclic voltammetry of a WE with different isolated areas of Au film (a); charge determination was carried out by an under-peak integration (an upper half of the panel is zoomed-in by $100^{\times}$).

is the Avogadro number. Considering that all Au surface atoms are oxidized to $Au(OH)_3$ during 5 min of oxidation at the potential of Burshtein minimum, cathodic charge density $\sigma_t \equiv 3\frac{\varphi_s}{N_a}F = 0.483$ mC/cm^2 (for a three electron process) would be required to reduce such monolayer of $Au(OH)_3$ according to the reaction: $Au(OH)_3 + 3e^- = Au + 3OH^-$; here F is the Faraday constant. We used this surface charge density $\sigma_t = 0.483$ mC/cm^2 (corresponding to the ideal atomically "flat" surface) for the estimation of the surface increase factor. The value ~ 0.48 mC/cm^2 is larger than the empirically determined 0.4 mC/cm^2 value [16] which, most probably, reflects the fact that actually not all gold surface atoms are converted to $Au(OH)_3$ due to steric constraints which arise during restructuring of Au surface in the course of anodic oxidation.

Integration of the I-V peaks to determine the charge was carried out by polynomial fitting of the peak and an under-curve integration with the built-in Voigt function using Origin software. Similar values were obtained by using potentiostat/galvanostat software.

2.2 Ripple fabrication and characterization

Ripples were fabricated using ultrashort laser pulses (∼150 fs) on the surface of different dielectric materials including SiC, Al_2O_3, GaP, glass and synthetic diamond substrates. The high refractive index, n, substrates are used for creation of small ripple periods $\Lambda \approx \lambda/n/2$ via a sphere-to-plane evolution of sub-surface breakdown [23]; also, a high melting temperature of sapphire and SiC facilitated recovery of nano-rough surface without melt-smoothing of the surface. Laser beam of $\lambda = 800$ nm wavelength was focussed on the optically flat substrate

surface using high numerical aperture ($NA = 0.7$) objective. Substrate was moved by linear stages (Aerotech Inc.) with respect to the stationary laser focal spot to create 200×200 μm^2 areas by direct laser writing. Nitrogen gas was purged on the surface of the substrate to remove debris, otherwise accumulating on the surface and preventing ripple fabrication on large areas. Fabrication was performed in air at ambient atmospheric conditions. After fabrication ripple substrates were ultrasonically cleaned in acetone, ethanol and deionised water to remove residual debris. The cleaned samples were further coated by different thickness of gold using magnetron sputtering (AXXIS, Kurt J.Laser Company), a 5 nm titanium sublayer was deposited on sapphire substrate to increase adhesion of the gold. Morphology of the laser nanotextured surfaces was inspected by scanning electron microscopy (SEM).

3 Results

3.1 Surface area measurement

To compare the real surface area S_r with a geometrical footprint S_g, voltammogram (Fig. 1) of a known S_g has to be measured. Figure 2(a) shows schematically connections used for the cyclic voltammetry. The working electrode WE was connected to a contact pad (CP in Fig. 2(a)), which was in direct electrical connectivity to an active surface of geometrical area S_g via a narrow ~ 10 μm wide conductive bridge. The area under investigation was electrically isolated from the rest of the Au-coated substrate by ablation of Au (Fig. 2(b),(c)) using the same fs-laser beam as for ripple fabrication. Since it is difficult to control an immersion depth of the WE in a standard cell, part of the channel can be immersed into electrolyte and increase the actual S_g area. The bridge area is around $0.01 \times 10 = 0.1$ mm^2 causing insignificant error for WE areas above 10 mm^2. In this work, limits of surface area measurements were tested down to 0.01 mm^2, where the bridge area induced error becomes significant. To avoid this problem, central part of the conductive bridge was isolated from contact with an electrolyte using a nail polish (Fig. 2). The total S_g area including the bridge region was precisely measured under the microscope (Fig. 2(b)).

Using the proposed method of charge determination, the real surface area can be measured from geometrical footprint as small as 0.01 mm^2 with a high accuracy $\sim$95% as shown in Fig. 3(a). Such areas are typical for SERS measurements in microscopy based setups. For accuracy measurements cover glass samples, coated by 30 nm of gold by magnetron sputtering, were used. Error was calculated as a relative standard deviation for the surface increase factor f_{si}, which was defined (Eq. 1) as a ratio between the real and geometrical footprint surface: $f_{si} = S_r/S_g$. The real surface area on a glass substrate, coated by 30 nm Au was only $\sim$ 20 % higher compared to the geometrical footprint $f_{si} = 1.22 \pm 0.06$. For each S_g value, three samples were prepared and measured under identical conditions. Each point on the plot in Fig. 3(a) represents the average f_{si} value, calculated from 3 similar samples. Relative standard devia-

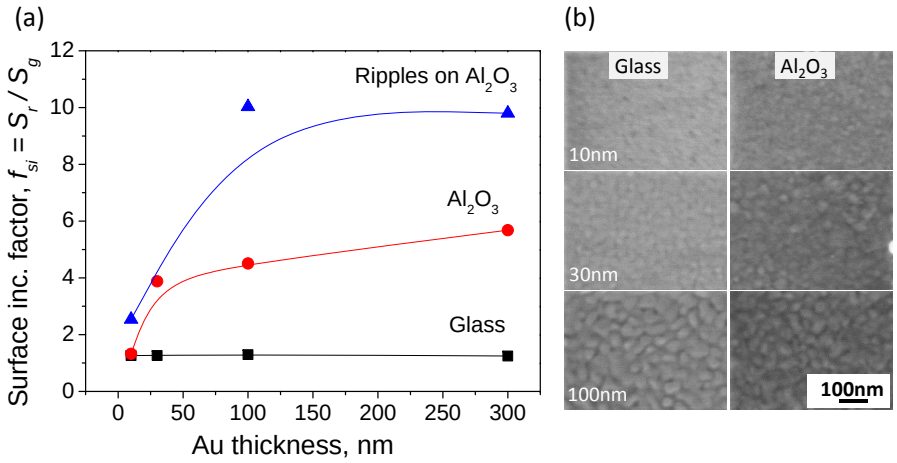

Figure 4: (a) Surface increase factor f_{si} as a function of Au thickness on different substrates: flat sapphire, ripples on sapphire and cover glass. Lines are shown as eye guides. (b) SEM images of glass and flat sapphire substrates coated by Au of different thickness 10, 30 and 100 nm. The same scale bar used for all images.

tion between samples with the same S_g was even lower, < 2 %. Figure 3(b) show cathodic peaks, which were used for the calculations of real surface area S_r shown in Fig. 3(a). Graph is split into two parts to show cathodic peaks measured from small and large areas of WEs.

It was found that the real surface area of Au on sapphire substrate can be increased by depositing thicker coating (Fig. 4(a)). Laser fabricated ripples additionally increase the surface area by factor of $\sim$2 independent on the Au thickness. For Au coatings above 100 nm, ripples on sapphire caused up to a tenfold increase of the surface area. Interestingly, the real surface area on a Au coated glass substrate was close to the geometrical footprint and did not increase with Au thickness.

SEM images show that a granular size of coating increases with thickness of Au layer for both glass and sapphire in a very similar way (Fig. 4(b)). An initial surface roughness may play a role, however, the glass and sapphire surfaces were of a 1-2 nm roughness. The real surface area is determined by cyclic voltammetry and is used here to compare performance of different SERS substrates. More subtle intricacies of surface morphology due to the granular pattern, nanoroughness, porosity of Au coating made by magnetron sputtering would require further studies. Obviously, surface tension is playing a role and thermal conditions of the coating deposition. The case presented here corresponds to the most popular room temperature sputter-deposition of Au for SERS sensors.

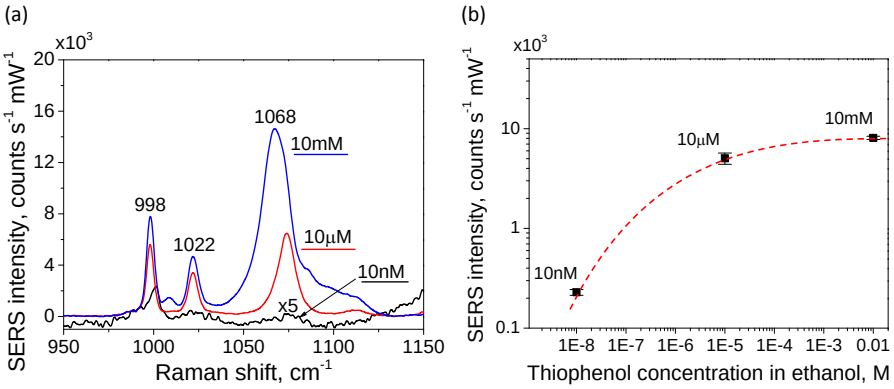

Figure 5: SERS intensity as a function of thiophenol concentration measured on sapphire ripples coated by 100 nm Au. (a) SERS spectra (10 nm spectra multiplied $5^{\times}$ for clearity), (b) average peak height of 998, 1022 and ∼1070 cm^{-1}, notice log-log scale. Conditions: $\lambda_{ex} = 633$ nm, $NA = 0.75$, 10 s acquisition time, $P = 1$ mW.

3.2 SERS measurements on ripples

The SERS intensity increase with thickness of Au layer deposited on ripples was previously demonstrated [14,24]. An increase of the actual surface area [14] and a higher reflectivity [24] were suggested to explain the augmented SERS intensity. It was shown that due to increased reflectivity, when Au thickness increases from 10 to 100 nm, SERS signal increased $\sim 3^{\times}$ times at 633 nm excitation wavelength. The SERS intensity dependence on thickness of Au coating varies for different analytes and on the coating deposition method, however, an increase of 6-$10^{\times}$ was following an Au thickness from 10 to 100 nm [14,24]. The reflectivity increase by $3^{\times}$ does not fully accounts for the higher SERS intensity. Here we give an experimental evidence that the actual surface area on ripples increases $\sim 5^{\times}$ times for the same Au thickness increase (from 10 to 100 nm). This correlates with the SERS signal due to increased number of Raman scatters (the analyte molecules) and an increased number density of the hot-spots.

Figure 5 shows SERS intensity dependence on concentration of thiophenol in solution; SERS substrates were immersed into the solution to form a self assembled monolayer on Au coating. Average of spectra measured at three random locations on SERS substrate are plotted for each thiophenol concentration (Fig. 5(a)); note, that spectrum of 10 nM is multiplied $5^{\times}$ times for clarity. It shows a clear evidence that SERS intensity increases with concentration. Laser nano-textured - ripple coated - sapphire SERS substrates, had 100 nm of Au film and were immersed into solutions of different thiophenol concentrations: 10 nM, 10 μM and 10 mM for 8 hours to allow enough time for binding to the Au surface. After the incubation, substrates were rinsed with ethanol to remove any access thiophenol molecules that did not absorb to gold.

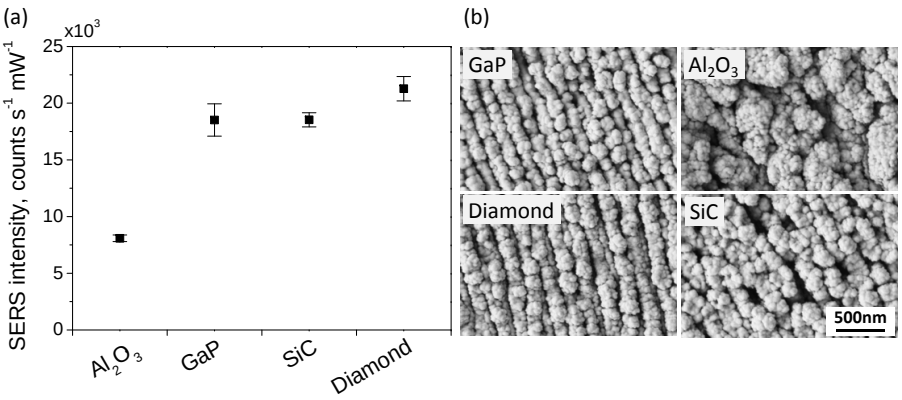

Figure 6: (a)SERS intensity of thiophenol as a function on substrate material coated by 100 nm Au. SERS measurement conditions: $\lambda_{ex} = 633$ nm, $NA = 0.75$, 10 s acquisition time, $P = 1$ mW. (b) SEM images of ripples, formed by 800 nm/150 fs pulses under a $NA = 0.7$ focussing conditions; the same scale bar for all images.

To quantitatively compare SERS intensity, the average peak height values of three distinct features at 998, 1022 and ∼1070 cm^{-1} were measured for each concentration (Fig. 5(b), notice the log-log scale). For concentration change between 10 nM and 10 μM ($10^{3\times}$) SERS intensity increased by $25^{\times}$, however between 10 μM and 10 mM (also a factor of $10^{3\times}$), an increase was only $\sim 1.6^{\times}$. This indicates, that at low concentrations ∼10 nM a uniform self-assembled monolayer was not formed in agreement with the Langmuir adsorption on gold surface [12].

The intensity of SERS was compared on different substrates fabricated using ultra-short laser pulses and coated by 100 nm gold. On GaP, SiC, and synthetic diamond it is on average $2.4^{\times}$ higher as compared to sapphire (Fig. 6(a)). This is, most probably, related to a less ordered and larger size structures formed on sapphire surface recognizable in SEM images in Fig. 6(b). Sapphire has the smallest refractive index of $n \simeq 1.7$ at 800 nm among the used substrates and correspondingly the ripple period is the largest. The same sample preparation protocol was followed for the 10 mM concentration of thiophenol for all the substrates shown in Fig. 6.

3.3 Surface area of a solar cell

Measurement of the actual surface area of solar cells can be carried out by the above demonstrated method for the SERS ripple micro-sensors [25]. Figure 7 shows the surface area determined using the cathodic charge measurement for planar and textured commercial c-Si solar cells. Planar solar cells show $1.4^{\times}$ and textured $3.1^{\times}$ times increase of the surface area compared to the geometrical footprint. Ripples could be used to improve charge collection and mechanical

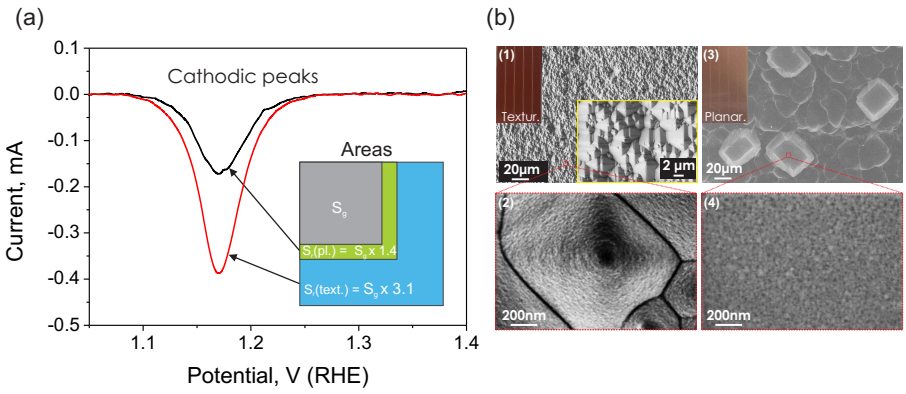

Figure 7: (a) Cathodic peaks of planar and textured c-Si solar cell, coated by 35 nm Au, measured at 0.01 V/s scan rate. Inset shows relative area increase for the planar and textured cell, which is $1.4^{\times}$ and $3.1^{\times}$ times higher, respectively, as compared to the atomically flat Au surface. (b) SEM images of the Au coated textured (1,2) and planar (3,4) c-Si solar cells. Random pyramids with a feature size of 1-6 μm are present on the surface of textured cells.

contact adhesion after fs-laser ablation of Si_3N_4 antireflection coating [26].

For solar cells the active surface area is one of the key factors determining their performance. Higher performance crystaline Si solar cells (c-Si) have nanotextured surfaces to collect more light by redirecting it to the solar cell at larger angles, which increases absorption. On the other hand, increased surface area introduces more losses due to surface recombination of photo-generated $e-h$ pairs. Ability to accurately measure real surface area may help in optimizing morphology of surface nano-texture for solar cell. Shadowing effect from the surface contacts (bus bars and fingers) is reducing a solar collection area. The most efficient solar harvesting solutions use sub-surface charge collection to reduce shadowing. Also, very same surface ripples are considered for better surface adhesion and charge collection when surface contacts are used [26].

4 Conclusions

A method to directly measure a surface area of laser-ablated surfaces used in SERS sensing is demonstrated. The method allows to correlate surface density of the hot-spots causing SERS enhancement, nano-roughness, and surface area. Direct measurement of surface area shows that the ripple-covered regions has up to tenfold larger surface area on sapphire. All the experiments were carried out with sputtered Au films which are known to be more nano-rough and porous as compared to thermally or ion-beam evaporated films. All the measurements were carried out on Au films thick enough to form a continuous film since only then the surface area determination can be compared with SERS. Thermal

treatment of Au-coated surfaces can be used to alter roughness and even cause dewetting and island formation of thin films. Those morphological modification can be traced using the method proposed here.

The revealed proportionality between SERS intensity and surface area is expected to be applicable for structures with aspect ratio below two $f_{ar} < 2$ since for $f_{ar} \gg 2$ such as observed in black-Si [27], SERS becomes very sensitive to the focusing height on tips of black-Si needles [28]. The presented method can be used to measure surface area of electrically continuous coatings even on nano-textured surfaces with features of aspect ratio $f_{ar} \sim 10$ which can be coated with an electrically conductive (a fully percolated) Au film [27]. The method is demonstrated for small sensing SERS micro-pads as well as for silicon solar cells and can be used for electrochemically controlled on-chip SERS [29].

Acknowledgements

Support via Australian Research Council DP120102980 grant and a collaborative project with Altechna Ltd. are gratefully acknowledged. We are grateful to Kęstutis Juodkazis for the guidance through setting up electrochemical experimental and surface charge determination and to Paul R. Stoddart for access to Raman microscope and discussions. RB made and characterized samples and carried out electrochemical measurements together with FN, JJ developed methodology of electrochemical measurements, SJ initiated the study. All the authors contributed to writing and editing of the manuscript.

References

[1] K. W. Kho, C. Y. Fu, U. S. Dinish, and M. Olivo, "Clinical SERS: are we there yet?," *J. Biophoton.* **4**(10), pp. 667 – 684, 2011.

[2] M. Moskovits, "Surface-enhanced Raman spectroscopy: a brief retrospective," *J. Raman Spectrosc.* **36**, pp. 485–496, 2005.

[3] K. Juodkazis, J. Juodkazytė, P. Kalinauskas, E. Jelmakas, and S. Juodkazis, "Photoelectrolysis of water: Solar hydrogen - achievements and perspectives," *Opt. Express: energy express* **18**, pp. A147–A160, 2010.

[4] M. Fleischmann, P. J. Hendra, and A. J. McQuillan, "Raman spectra of pyridine adsorbed at a silver electrode," *Chem. Phys. Lett.* **26**(2), pp. 163–166, 1973.

[5] H. X. Xu, J. Aizpurua, M. Käll, and P. Apell, "Electromagnetic contributions to single-molecule sensitivity in surface-enhanced Raman scattering," *Phys. Rev. E* **62**, pp. 4318 – 4324, 2000.

[6] D. A. Genov, A. K. Sarychev, V. M. Shalaev, and A. Wei, "Resonant field enhancements from metal nanoparticle arrays," *Nano Lett.* **4**(1), pp. 153–158, 2004.

[7] J. B. Lassiter, H. Sobhani, J. A. Fan, J. Kundu, P. N. F. Capasso, and N. J. Halas, "Fano resonances in plasmonic nanoclusters: Geometrical and chemical tunability," *Nano Lett.* **10**(8), pp. 3184–3189, 2010.

[8] Y. Sonnefraud, N. Verellen, H. Sobhani, G. A. Vandenbosch, V. V. Moshchalkov, P. V. Dorpe, P. Nordlander, and S. A. Maier, "Experimental realization of subradiant, superradiant, and Fano resonances in ring/disk plasmonic nanocavities," *ACS Nano* **4**(3), pp. 1664–1670, 2008.

[9] E. Zachariah, A. Bankapur, C. Santhosh, M. Valiathan, and D. Mathur, "Probing oxidative stress in single erythrocytes with Raman tweezers," *J. Photochem. and Photobiol. B: Biol.* **100**, pp. 113 – 116, 2010.

[10] A. J. Hobro, A. Konishi, C. Coban, and N. I. Smith, "Raman spectroscopic analysis of malaria disease progression via blood and plasma samples," *Analyst* , p. online DOI: 10.1039/C3AN00255A, 2013.

[11] K. Ueno, S. Juodkazis, V. Mizeikis, K. Sasaki, and H. Misawa, "Clusters of closely spaced gold nanoparticles as a source of two-photon photoluminescence at visible wavelengths," *Adv. Mat.* **20**(1), pp. 26 – 29, 2008.

[12] Y. Yokota, K. Ueno, S. Juodkazis, V. Mizeikis, N. Murazawa, H. Misawa, H. Kasa, K. Kintaka, and J. Nishii, "Nano-textured metallic surfaces for optical sensing and detection applications," *J. Photochem. Photobiol. A* **207**, pp. 126 – 134, 2009.

[13] Y. Nishijima, J. B. Khurgin, L. Rosa, H. Fujiwara, and S. Juodkazis, "Randomization of gold nano-brick arrays: a tool for SERS enhancement," *Opt. Express* **21**(11), pp. 13502–13514, 2013.

[14] R. Buividas, P. R. Stoddart, and S. Juodkazis, "Laser fabricated ripple substrates for surface-enahnced Raman scattering," *Annalen der Physik* **524**(11), pp. L5 – L10, 2012.

[15] J. M. Doña Rodríguez, J. A. Herrera Melián, and J. Pérez Peña, "Determination of the real surface area of pt electrodes by hydrogen adsorption using cyclic voltammetry," *Journal of Chemical Education* **77**(9), p. 1195, 2000.

[16] A. Michri, A. Pshenichnikov, and R. K. Burshtein, "Determination of the true surface of smooth au electrodes," *Elektrokhimiya* **8**(3), pp. 364–366, 1972.

[17] S. Trasatti and O. Petrii, "Real surface area measurements in electrochemistry," *Pure and applied chemistry* **63**(5), pp. 711–734, 1991.

[18] D. Rand and R.Woods *J. Electroanal. Chem.* **31**, p. 29, 1971.

[19] K. Juodkazis, J. Juodkazytė, T. Juodienė, V. Šukienė, and I. Savickaja, "Alternative view of anodic surface oxidation of noble metals," *Electrochimica acta* **51**(27), pp. 6159–6164, 2006.

[20] K. Juodkazis, J. J, B. Šebeka, and L. A, "Evaluation of the thickness of au(iii) hydroxide surface layer anodically formed on gold electrode," *Chemija* **9**, p. 46, 1998.

[21] H. Angerstein-Kozlowska, *Comprehensive Treaties of Electrochemistry*, vol. 9, Plenum Press, New York and London, 1985.

[22] J. R. Anderson, *Structure of metallic catalysts*, Academic Press, 1975.

[23] R.Buividas, L. Rosa, R. Šliupas, T. Kudrius, G. Šlekys, V. Datsyuk, and S. Juodkazis, "Mechanism of fine ripple formation on surfaces of (semi)transparent materials via a half-wavelength cavity feedback," *Nanotechnology* **22**, p. 055304, 2011.

[24] A. Chou, E. Jaatinen, R. Buividas, G. Seniutinas, S. Juodkazis, E. L. Izake, and P. M. Fredericks, "SERS substrate for detection of explosives," *Nanoscale* **4**(23), pp. 7419 – 7424, 2012.

[25] R. Buividas, N. Fahim, B. Jia, M. Gu, and S. Juodkazis, "Accurate measurement of the surface area of solar cells," in *book of abstracts, Solar 2012, Melbourne*, 2012.

[26] R. Buividas, M.Mikutis, T. Kudrius, A. Greičius, G. Šlekys, and S. Juodkazis, "Femtosecond laser processing - a new enabling technology," *Lith. J. Phys.* **57**(4), pp. 301–311, 2013 (in press).

[27] A. Žukauskas, M. Malinauskas, A. Kadys, G. Gervinskas, G. Seniutinas, S. Kandasamy, and S. Juodkazis, "Black silicon: substrate for laser 3D micro/nano-polymerization," *Optics Express* **21**(6), pp. 6901–6909, 2013.

[28] G. Gervinskas, G. Seniutinas, J. S. Hartley, S. Kandasamy, P. R. Stoddart, N. F. Fahim, and S. Juodkazis, "Surface-enhanced Raman scattering sensing on black silicon," *Annalen der Physik* , p. online DOI 10.1002/andp.201300035, 2013.

[29] M. M. Islam, K. Ueno, S. Juodkazis, Y. Yokota, and H. Misawa, "Development of interdigitated array electrodes with SERS functionality," *Analytical Sciences* **26**, pp. 13–18, 2010.